

In-situ Submarine Pipeline Inspection Based on the Structured Light in the High-turbidity Condition

Hai Zhu^a, Jiawang Chen^{c,*}, Yuan Lin^a, Peng Zhou^a, Peiwen Lin^a, Xiaoqing Peng^a, Haonan Li^a, Kaichuang Wang^a, Jin Guo^a, Xueyu Ren^a, Han Ge^a, Zhonghui Zhou^a, Yuping Fang^a, Zhenjun Jiang^a, Feng Gao^a, Wendi Dai^a, Xuehua Chen^b, Guoming Cao^b, Honghe Li^b, Xu Gao^b, Zhaoqiang Sun^b

^a Institute of Ocean Engineering and Technology, Zhejiang University, Zhoushan, Zhejiang 316021, China

^b Pipe China Eastern Oil Storage and Transportation Co. Ltd., ZhouXu, Jiangsu 221008, China

^c Donghai Laboratory, Zhoushan, Zhejiang 316021, China

*Corresponding author. E-mail: arwang@zju.edu.cn, Tel: +8618667171179, Address: 101 Haigong Building, Zhoushan Campus, Zhejiang University, Dinghai District, Zhoushan City, Zhejiang Province, China

ABSTRACT The safety of submarine pipelines is crucial to offshore oil and gas operations. This study developed an unmanned submarine light-scanning mapping system that combines structured light technology with a large-scale underwater dry chamber, enabling precise in-situ external pipeline inspection in the high-turbidity condition. A sophisticated structured light scanning driving system(SLSDS) for precise motion control of the structured-light scanner is designed, combined with the motor synchronous drive technology and tailored strategies for pipeline mapping, leading to a seamless full scan in a single deployment. In addition, a shipboard electric control subsystem(SECS) is set up to provide an integrated solution for power supply, sensing, communication, and control. The proposed dry-cabin mapping system has been successfully applied in the Zhoushan sea area offshore, demonstrating its potential to be widely used in the offshore area with poor-visibility underwater conditions.

KEYWORDS submarine pipeline inspection, underwater dry-cabin, structured light, shipboard electric control subsystem, synchronal drive

1. Introduction

Submarine pipeline inspection techniques are developed to locate pipeline defects for carbon reduction, environmental protection, and pipeline integrity management[1–5]. The prevalent method is the internal inspection technique with detectors inside the pipelines[6]. Direct mechanical measurement, magnetic flux leakage (MFL) detection, and ultrasonic test (UT) are widely used technologies[7]. Magnetic flux leakage (MFL) detectors use magnets to introduce magnetic flux into the pipe wall or weld seams. Sensors are placed between the two magnetic poles to detect various MFL phenomena caused by wall thinning or corrosion[8–10]. This technique is employed in most international pipeline inspections[7]. Ultrasonic (UT) detectors, on the other hand, utilize the time difference between reflected waves from the inner and outer surfaces of the pipeline to measure wall corrosion and thickness[11,12]. However, its detection requires a liquid environment, which imposes certain limitations on its usage[7]. Nevertheless, the internal inspection techniques have their limitations on navigation, motion control as well as obstacle avoidance of the detectors. Also, a halt of the pipeline system is essential for such detection to be carried out, leading to a high cost[13,14].

Considerable effort has been made to develop several external inspection methods as a complement[15–18]. In contrast to internal inspections, external inspections offer the distinct advantage of non-intrusiveness, substantially reducing their impact on the normal operation of the pipeline network[19,20]. There are roughly three types of outer detection methods, namely, (1) a large-scale inspection employing conventional geophysical detecting instruments such as sub-bottom profilers (SBP)[21], multibeam systems (MBS)[22], side-scan sonar systems (SSS)[23–25], and magnetometer (MAG)[26,27], and (2) contact measurement methods including point contact measurement (PCM)[28], Magnetic Particle Testing(MPI)[29,30], and (3) close range small-scale non-destructive detection (NDT) methods involving visual testing (VT), ultrasonic test (UT) [31,32], eddy-current test (ECT)[33], digital radiographic testing (DRT)[34], alternating current field measurement (ACFM)[35–37], to name a few[36].

Nevertheless, the external inspection method also has deficiencies. For example, the geophysical inspection method has limited accuracy when applied on pipelines, which cannot clearly identify small pits or cracks that allow for precise repair. On the other hand, for the contact measurement methods and close-range NDT methods, detection depends very much on the proficiency of divers or underwater vehicles, as well as the working conditions, and underwater visibility is considered to be the main factor. Consequently, a high-accuracy and reliable detection technique with a novel conception is desired to address these issues, especially in hostile underwater conditions (e.g., high-turbidity conditions).

The vital objective of pipeline surface defect assessment is to obtain the depth information accurately. As an advanced deep-sensing technology, the structured light(SL) technique, through the projection and analysis of structured light patterns or array of dots, enables the precise acquisition of the surface topography of the object [38–43]. Structured light technology is widely used in many fields due to its good 3D reconstruction ability and real-time performance, and a notable example is

manufacturing encompasses 3D measurements, quality control, and process optimization [44–47]. Furthermore, its utility extends to diverse fields. Several recent endeavors have employed structured light technology for pipeline defect detection [48,49]. However, its potential to diagnose the submarine pipelines remains unexplored due to the challenges posed by the submarine environment's interference.

In this study, an unmanned detection device based on the 3D structured light for submarine pipeline defect mapping is developed. The device incorporates an underwater dry chamber, creating an air-filled space, thereby enabling reliable optical measurements irrespective of seawater visibility. The motion control of the scanner is remotely implemented through the integration of SLSDS and SECS, improving the measuring accuracy and stability through the motor synchronous drive technology. This innovative approach ensures comprehensive and efficient inspection of the pipeline's surface for defects. Additionally, leveraging the SECS, a complete shipborne operation method is established, significantly reducing costs associated with human divers.

2. System Design and Manufacture

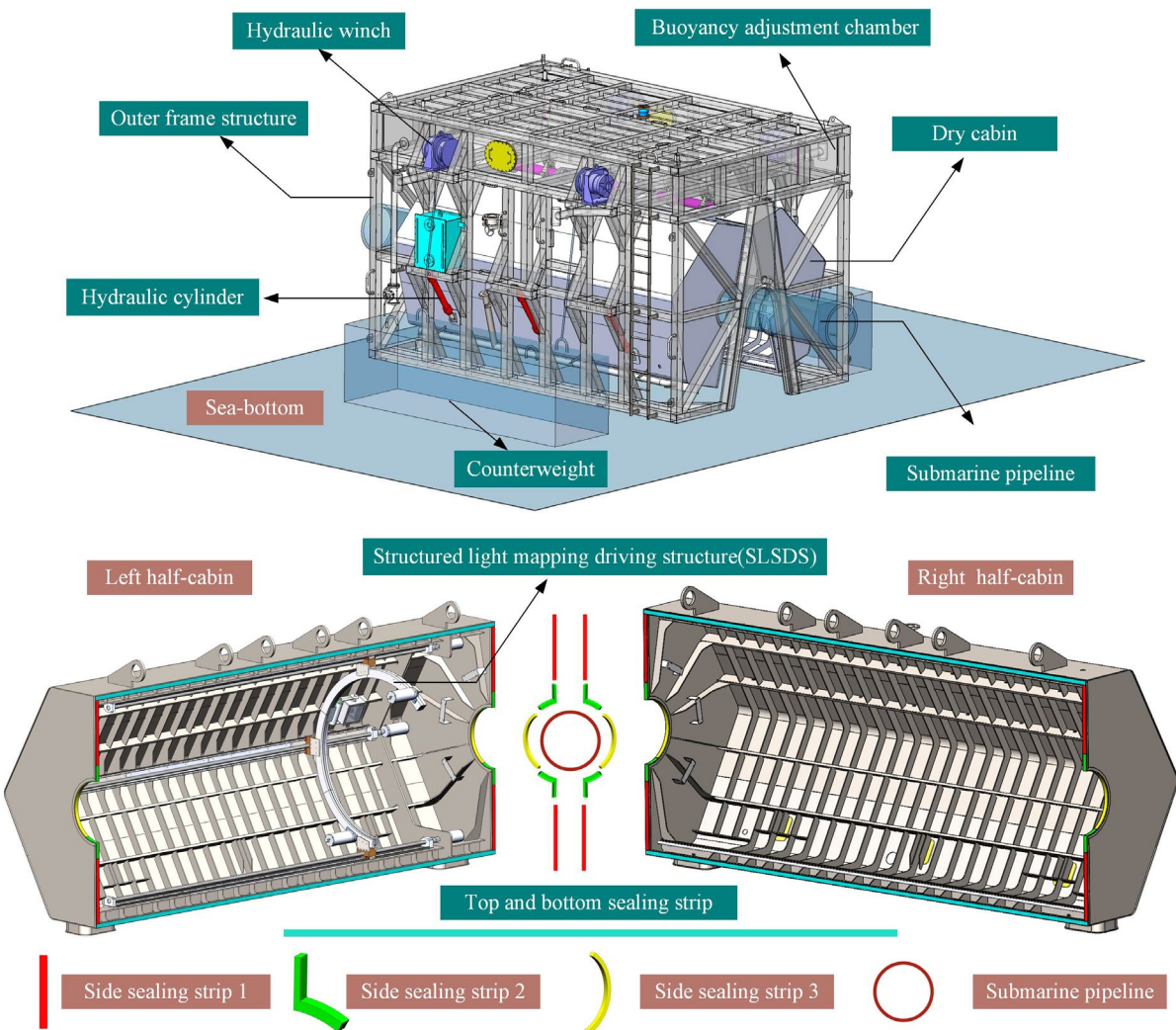


Fig. 1. Submarine pipeline defect external inspection equipment based on the dry cabin and structured light

The overall structure of the structure-light mapping equipment for submarine pipelines is shown in Figure 1. The essential components encompass the dry cabin, the SLSDS, and the outer frame structure. Additionally, the equipment is complemented by a range of auxiliary devices, such as hydraulic winches, pumps, hydraulic cylinders, and a buoyancy adjustment chamber, among others, all working in synergy to ensure optimal functionality and efficiency. A submersible pump and a pneumatic diaphragm pump are installed inside the dry cabin to discharge the seawater during the medium replacement (from seawater to air). The SLSDS is installed inside the dry cabin, combined with the SECS, realizing the linear and circular scanning motion of the structure-light scanner.

During the operation, the facility is deployed from the shipboard and is precisely positioned on the pipeline with the aid of divers. Subsequently, the cabin is securely closed and sealed around the pipe, following which the seawater within the cabin is replaced with dry air. Upon activation, the structured-light scanner inside the cabin is remotely controlled to comprehensively scan the entire pipeline surface, facilitating the 3D reconstruction of the target pipe. Detailed specifications and capabilities of the developed facility are provided in Table 1.

Table 1 The Detailed specifications and capabilities of the submarine pipeline defect external inspection equipment

Parameters	Value/ requirements	Parameters	Value/ requirements
Maximum mapping length	5685mm	Maximum data post-processing time (complete 3D image)	6 hours
Applicable water depth, up to	33msw	Applicable bending angle of a 762mm straight pipeline, up to	15degrees
Mapping accuracy, up to	0.1mm	Applicable diameter of the straight pipeline, up to	880mm
3D data model requirements	editable	Control requirements of the mapping process	remotely & real-time

2.1 Structure design of the SLSDS

The SLSDS is designed for remote operation, obviating the necessity for human intervention. The scanning and control of the underwater environment are performed through the ship-mounted control interface. The core objectives of this subsystem entail precise regulation of the structured-light scanner's angle and position. During the design of the driving subsystem, other limiting factors to be considered include the requirements for scanning submarine pipeline defects (as discussed earlier), achieving the encirclement and disconnection of the pipeline, ensuring the synchronization and stability of the driving mechanism, and facilitating remote visualized operation. The designed SLSDS is illustrated in Figure 2.

The SLSDS consists of a motion control subsystem and a 3D structured-light scanner, where the latter serves as the core component for submarine pipeline scanning. Its fundamental principle is to replace one data source of binocular vision with a structured light emitter, which projects light patterns with distinct features onto the measured object[50–52]. These patterns are then matched and stitched together by a high-definition camera, thus forming complete 3D point cloud data[41,53].

Commonly used structured light projection methods include Sequential Projection Techniques, Full-Frame Spatially Varying Color Patterns, Stripe Indexing (Single Shot), and Grid Indexing: 2D Spatial Grid Patterns[40,54–59]. Structured light equipment based on optical triangulation and phase shifting is widely adopted. In these methods, pre-designed patterns with special structures, such as discrete spots, stripe light, and coding structured light, are projected onto the surface of a 3D object. Another camera is used to observe the imaging distortion on the 3D surface. Suppose the projected pattern on the object's surface is flat. In that case, the observed structured light pattern is similar to the projected one with no deformation, except for some scaling variations based on the distance. However, if the object's surface is not flat, the observed structured light pattern will deform differently due to the object's geometric shape and distance. The algorithm can calculate the measured object's 3D shape and depth information by using known structured light patterns and observed deformation.

Given the limited scanning range of the 3D structured-light scanner in terms of angles and distances, enough degree of freedom is necessary to perform fine adjustments for scanning. The power supply of all the execution components depends on the shipboard electric control system since the motors, drivers, and scanners are not waterproof. Therefore, these components have separate sealed cabins designed, and vulcanized rubber is utilized to seal and pressure-protect all cables. Servo motors and stepping motors are the power source to ensure accuracy and output torque. Transparent materials are used on the light transmission side of the sealed cabin that the scanner lens faces. Tempered glass is selected as the transparent panel considering both transparency and strength. However, the influence of the refracted light path cannot be ignored, which will negatively affect image quality and accuracy. Nevertheless, the negative impact mentioned above is deemed acceptable according to practical measurements of this specific application scenario.

The shape characteristics of submarine pipeline sections, scanning requirements, and scanning system parameters determine the need for linear motion, circular motion, and small-angle rotation within the scanner. Linear motion for the scanner is achieved through a screw and nut mechanism, wherein the rotary motion of the screw is effectively transformed into linear motion to drive the scanner. The servo motors within the sealed cabin provide the necessary power for the rotation of the screw. Circular motion is realized by a gear-driven mechanism, employing an open-loop circular large gear as the driven object, which houses the installed scanner. A pair of small gears alternately drives the large gear, ensuring a continuous

and synchronized engagement of the gear pairs throughout the operation. Angular motion is accomplished through a chain-transmission system, with the necessary power supplied by a motor.

The Artec Leo is a structured-light scanner that sends out a known pattern of light and observes how it's deformed to calculate the geometry of an object. The essential characteristic parameters of Artec Leo are as follows:

Table 2 Technical specifications of Artec Leo

Parameters	Value	Parameters	Value
3D point accuracy, up to	0.1 mm	Working distance	0.35 – 1.2 m
3D resolution, up to	0.2 mm	Volume capture zone	160,000 cm ³
Hybrid geometry and texture tracking	Yes	3D light source	VCSEL
3D exposure time	0.0002 s	2D light source	White 12 LED array
2D exposure time	0.0002 s	Interface	Wi-Fi, Ethernet, SD card
Position sensors	Built-in 9 DoF inertial system	Angular field of view, H×W	38.5 × 23°

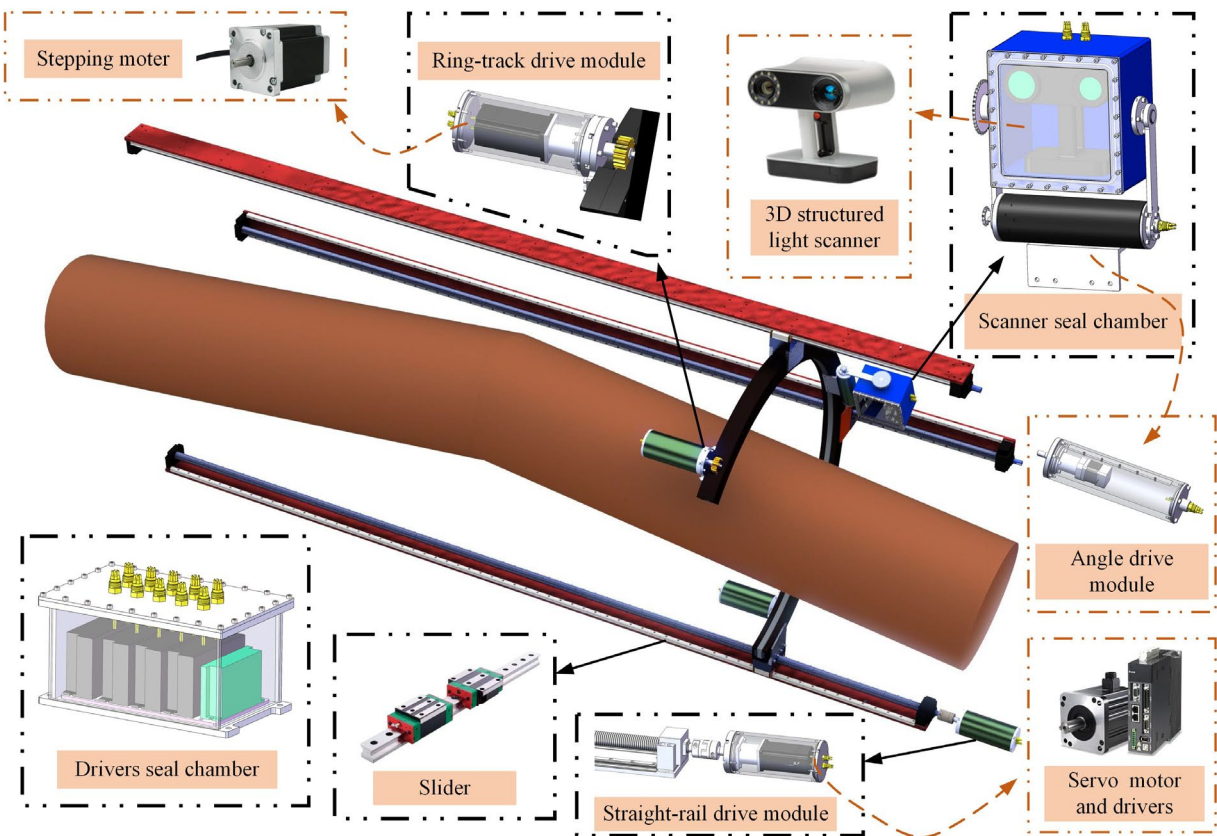


Fig. 2. Structured light scanning driving system (SLSDS)

The precise control of the servo and stepper motors, which serve as the power sources for the scanning system, relies on the upper computer control system and driver implementation. By inputting the speed and number of circles on the upper computer (Figure 5), the motor executes the preset action according to the input command. It provides feedback on the final status, such as whether it is in place or has a deviation of several circles. The operator can then make necessary adjustments based on the feedback.

2.2 Calculation of the different scanning strategies

Achieving comprehensive coverage of submarine pipelines during the inspection is a critical aspect that necessitates addressing challenges related to the scanning angle and overlapping requirements. To overcome these hurdles effectively, a multi-phase scanning approach is proposed. This strategy involves categorizing the scanning process into two primary

techniques, namely linear scanning and circular scanning, tailored to the unique characteristics of the submarine pipeline. Employing diverse scanning strategies based on the specific inspection scenario ensures the completion of full surface coverage, optimizing the overall inspection process.

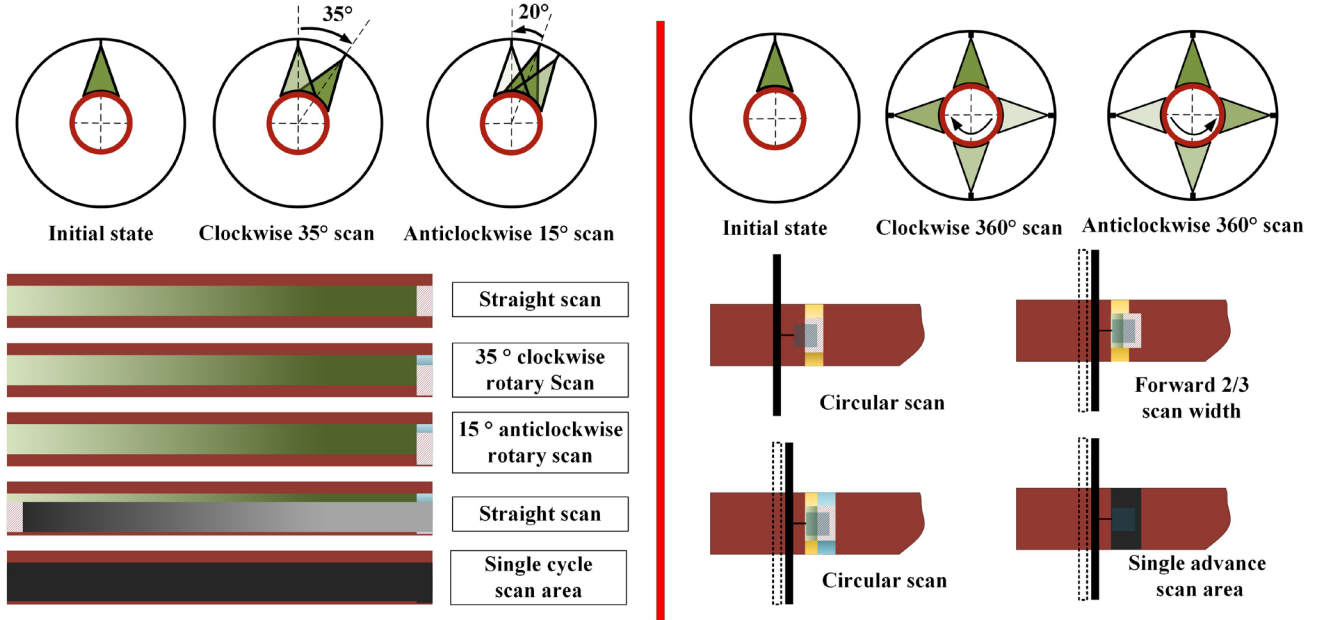


Fig. 3. Linear scanning (left) and circular scanning (right)

The field-of-view angle in the width direction of the 3D laser scanner is $\theta = 38.5^\circ$ and the field-of-view angle in the length direction $\mu = 23^\circ$. The minimum working distance supported is d_{min} , the max working distance d_{max} . Assuming that the distance from the projection plane to the structured light lens scanned by the structured-light scanner on the pipe is H and the distance H satisfies $d_{min} \leq H \leq d_{max}$; The scanning range is, therefore:

$$W = 2 * H * \tan \frac{\theta}{2}, \quad L = 2 * H * \tan \frac{\mu}{2} \quad (1)$$

According to the scanner data quality assurance principle: two consecutive scans must ensure more than one-third of the data coincidence. Assuming β represents half of the arc angle of the structured light projection surface on the surface of the pipeline. Therefore, according to the needs of the direct scan, the degree of coincidence between adjacent scans α should be satisfied:

$$\alpha \geq \frac{4}{3} \beta \quad (2)$$

Assuming D is the diameter of the open-loop circular large gear, d is the outer diameter of the submarine pipeline, r is the outer radius of the submarine pipeline, and l is the distance from the structured light lens to the open-loop circular large gear. Based on the analytic geometry, the following formulas can be obtained:

$$\beta = \arcsin \frac{H * \tan \frac{\theta}{2}}{r}, \quad H = \frac{D - d}{2} - l + (r - r * \cos \beta) \quad (3)$$

Within this project:

$$0 < \frac{H * \tan \frac{\theta}{2}}{r} < 1 \quad (4)$$

Therefore:

$$H = \frac{D - d}{2} - l + r - r \times \sqrt{1 - \left(\frac{H * \tan \frac{\theta}{2}}{r}\right)^2} \quad (5)$$

Converts to a quadratic equation of one variable as:

$$\left[1 + \left(\tan \frac{\theta}{2}\right)^2\right]H^2 + (2l - D)H + \left(l^2 + \frac{D^2}{4} - lD - r^2\right) = 0 \quad (6)$$

Therefore:

$$H = \frac{D - 2l \pm \sqrt{\left(2l - D\right)^2 - 4 * [1 + \left(\tan \frac{\theta}{2}\right)^2] \left(l^2 + \frac{D^2}{4} - lD - r^2\right)}}{2 * [1 + \left(\tan \frac{\theta}{2}\right)^2]} \quad (7)$$

Because:

$$L = 2 * H * \tan \frac{\mu}{\gamma}, \quad \beta = \arcsin \frac{H * \tan \frac{\theta}{2}}{r} \quad (8)$$

For the straight scan strategy, to ensure that the overlap between two scans is greater than $1/3$, the clockwise rotation angle should be slightly less than 2β , and the counterclockwise rotation angle should be marginally greater $2\beta/3$ to achieve a high-quality fusion of scanned data. For the circular scan strategy, the length of the advance is marginally less than L , and the next length of the back is marginally greater than $L/3$ to ensure the overlap of the two adjacent scans when scanning the ring.

2.3. Shipboard electric control system(SECS)

The SECS is shown in Fig 4, which system consists of several key components, including the control and scanning unit (upper computer, serial port server, motor driver, structured-light scanner), power supply and distribution unit (solenoid valve box, power distribution cabinet, and power distribution module), image acquisition unit (shipboard optical terminal, underwater optical terminal, underwater lamps, and webcams), and sensor unit (attitude sensor, depth gauge, tension sensor, cylinder displacement sensor, liquid level sensor, position switch).

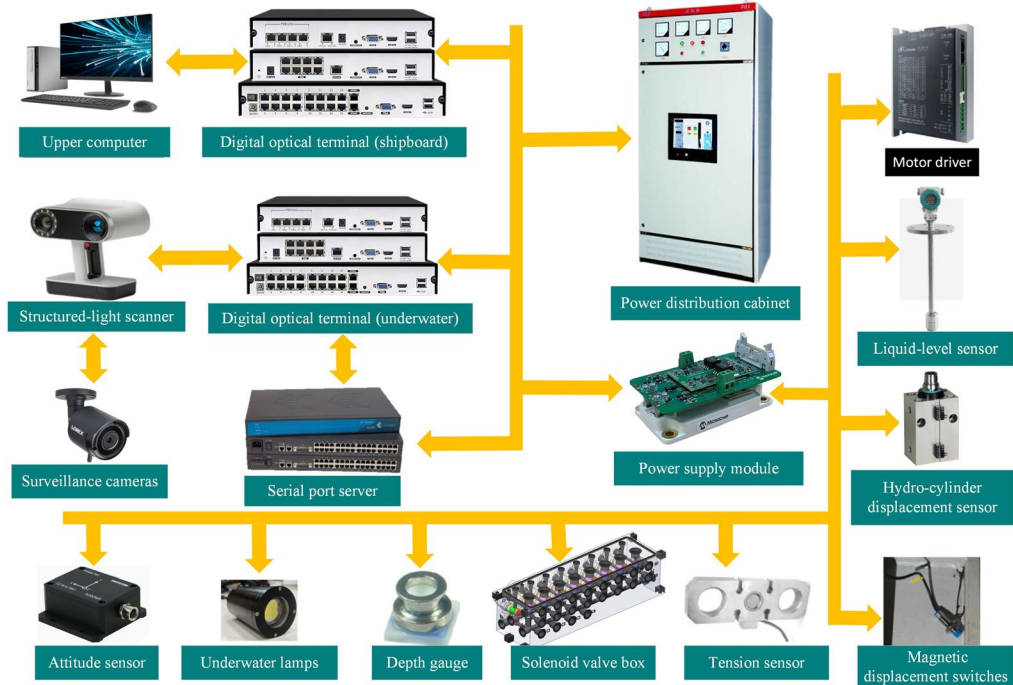


Fig. 4. Shipboard electrical control system for the submarine pipeline defect external inspection equipment

The control and scanning unit controls all subunits, including acquiring and transmitting data from sensor units, controlling motor speeds and revolutions for pipeline surface defect scanning, and uploading real-time 3D laser scanning data of the offshore pipeline shape. It also interfaces with the dry cabin image acquisition unit for video data feedback. The serial

port server provides eight serial ports to network port conversion through its built-in RS485 signal conversion to network signal port, with the ability to config different communication rates and port numbers for serial communication.

The power supply and distribution unit is responsible for providing power to all constituent parts and components of the device. It converts the distributed power supply into voltage values appropriate for each unit through its step-down module. It subsequently provides power to each unit through its respective control relay and circuit protection device. The power distribution cabinet has the responsibility of providing power to underwater high-voltage electrical appliances and provides corresponding protection functions for them (including the submersible pump, diaphragm pump, and hydraulic system). On the other hand, the power supply module is accountable for providing power to sensors and other low-voltage electrical appliances. At the same time, the solenoid valve box is charged with the responsibility of effecting hydraulic oil circuit switching.

The imaging acquisition unit is responsible for real-time monitoring of the interior of the dry chamber and the transmission of video data. The optical terminals are responsible for providing channels for the mutual conversion of the optical signals between the shipboard and underwater systems. The webcams and underwater lights provide real-time image information of the underwater dry cabin for the scanning device and serve as a basis for formulating motor control strategies during pipeline defect scanning. Twelve cameras are strategically positioned at different locations within the dry cabin to ensure comprehensive monitoring of the cabin's interior.

The sensor unit plays a crucial role in acquiring and transmitting all sensors' data, providing a reliable basis for decision-making for operators on board. Specifically, the attitude sensor and depth gauge are responsible for providing real-time attitude and equipment depth information during the underwater installation and recovery of the device, contributing significantly to the accuracy and precision of the measurement data. Moreover, the hydro-cylinder displacement sensor provides feedback on the opening and closing process of the compartment's dry compartments on the left and right sides. The tension sensors are designed to obtain the tightening and releasing actions of the four positioning hydraulic winches, thereby providing valuable tension data. Additionally, the liquid level sensor provides real-time feedback on the liquid level data of the buoyancy module and the dry cabin of the device. Finally, the position switch indicates whether the left and right compartments are in contact to achieve underwater sealing.

To achieve better mapping results, providing as much state data as possible about the submarine unmanned dry cabin can provide a rich and timely reference for issuing instructions for pipeline defect scanning is nesessary. As the core functional component of the SECS, the shipborne upper computer system is mainly responsible for obtaining the information in the dry cabin and performing underwater actions according to the situation, which is divided into the upper computer control interface and the upper computer monitoring interface. All data of the interface is collected and fed back in real-time.

The upper computer control interface is divided into several main display panels, as shown in Figure 5 and Table 3.



Fig. 5. Upper computer control interface (in Chinese)

Table 3 The detailed introduction of each panel of the upper computer control interface

Panel	Introduction
The attitude graphical display panel	Real-time graphical display of information of the equipment's pitch angle, yaw angle, and roll angle
Hydraulic winch and hydraulic cylinder control panel	Control the start and stop of the hydraulic winch and hydraulic cylinder, realizing the opening and closing of the dry cabin and fine distribution of counterweight gravity at four corners of the equipment
Module status display panel	Status display of various modules, including signal acquisition board, attitude sensor, depth gauge, and other sensors, in order to find out the failure of the above modules due to water leakage in the sealed chamber in time
Dry cabin surveillance cameras control panel	The monitoring system is equipped with 12 cameras, which are placed in different positions inside the dry cabin to ensure that the situation in the cabin can be fully displayed.
Dry cabin lighting control panel	Switch and brightness adjustment of 8 underwater lamps, which are placed in different positions inside the dry cabin to ensure that the dry cabin is fully illuminated.
Running status display panel	Display serial port information
Panel for linear motion	The control and display panel for driving SLSDS's servo motors of the linear motion, input the required number of motor turns and speed, obtain the accumulated position in real time, and judge whether the action is in place.
Panel for circular motion	The control and display panel for driving SLSDS's stepping motors of the circular motion, input the required number of motor turns and speed, obtains the accumulated position in real-time, and judges whether the action is in place.
Panel for small-angle motion	The control and display panel for driving SLSDS's stepping motors of the small-angle motion, input the required number of motor turns and speed, obtains the accumulated position in real-time, and judges whether the action is in place.
Depth and temperature display panel	The depth and temperature information display of the equipment

The upper computer monitoring interface is divided into several main display panels, as shown in Figure 6 and Table 4.

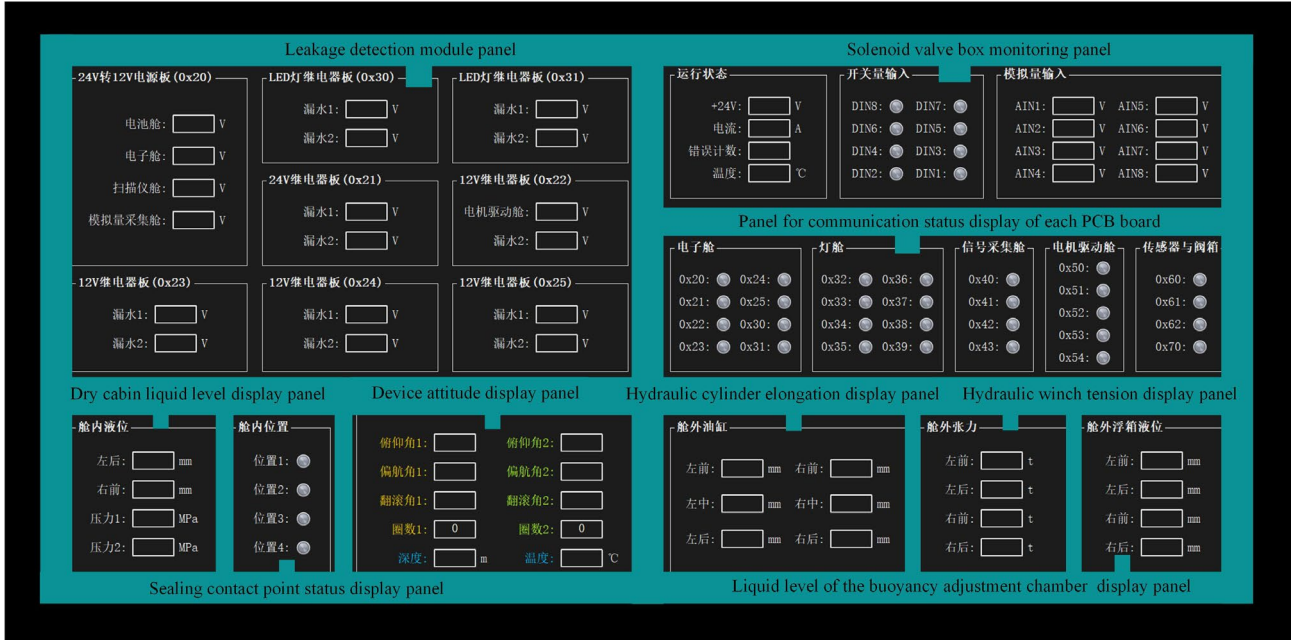


Fig. 6. Upper computer monitoring interface (in Chinese)

Table 4 The detailed introduction of each panel of the upper computer monitoring interface

Panel	Introduction
Leakage detection module panel	Check whether the circuit board of each functional module leaks water for timely maintenance. It mainly includes 12V and 24V power conversion circuits and lighting power supply boards. In addition, it also includes a power voltage display of battery-sealed cabin, scanner-sealed cabin, etc.
Solenoid valve box monitoring panel	Display the status of each path of the solenoid valve box, and include the feedback of temperature, current, voltage, and other information.
Panel for communication status display of each PCB board	Display the serial port information of the electronic chamber and monitor the working status
Dry cabin liquid level display panel	Two liquid level sensors are placed in different positions in the dry tank to evaluate the progress of drainage in the tank.
Device attitude display panel	Real-time display of pitch angle, yaw angle, and roll angle of the equipment and depth and temperature information display of equipment
Sealing contact point status display panel	Four magnetic displacement switches are placed on the sealing contact surface to judge whether the dry cabin is completely closed and guide whether the hydraulic cylinder at the corresponding position continues to extend.
Hydraulic cylinder elongation display panel	Six hydraulic cylinders are placed outside the dry cabin, respectively on the left and right sides of the dry cabin, with three on each side. This field shows its elongation length.
Hydraulic winch tension display panel	Four hydraulic winches are placed at four corners of the outer frame structure and connected with the counterweight, and their tension is shown here.
Liquid level of the buoyancy adjustment chamber display panel	Four liquid level sensors are placed in the buoyancy adjustment chamber to evaluate the liquid level in the tank.

2.4 Motor synchronous drive technology

- SLSDS driving unit

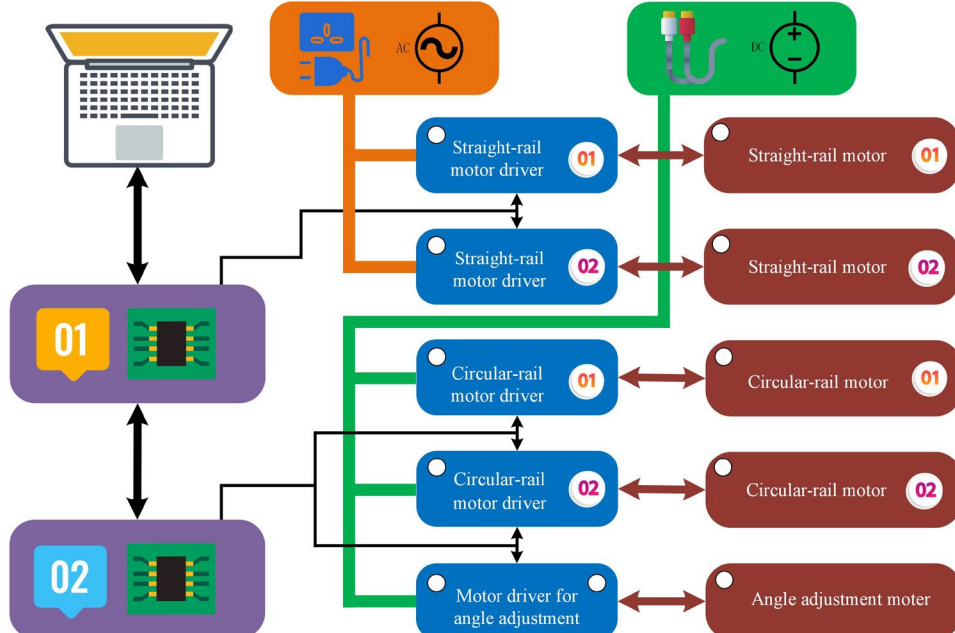


Fig. 7. Straight scan (left) and circular scan (right)

Based on the dry chamber approach, the scanning unit of the 3D precision scanning system for submarine pipeline deformation defects is governed by a sophisticated driving unit. As shown in Figure 7, control board 1, employing the RS485 bus, regulates linear motors 1 and 2 for their linear movements, while control board 2, also utilizing the RS485 bus, governs rotary motors 1 and 2, as well as the angle motor of the scanning unit. This architecture, with separate control boards for linear and rotary motors, enables synchronized control of the two motor sets. Leveraging a preconfigured control logic, the supervisory computer precisely regulates the speed and position of the linear motors, rotary motors, and the angle motor of the scanning unit, thereby facilitating a comprehensive 360-degree scanning coverage of the specific length of the submarine pipeline within the dry chamber.

- Closed-loop motor driving control

The scanning unit of the 3D precision scanning system for submarine pipeline deformation defects, based on the dry chamber approach, necessitates precise positioning along the axial direction of the submarine pipeline and accurate angular positioning along the radial direction. Moreover, the scanning unit requires alternating axial and radial movements, with adjustable velocities for linear translation and radial rotation to meet the operational demands. To address these functional requirements, we employ a servo control system with a three-loop control structure. The inner loop serves as the current loop, ensuring rapid response control of current and torque. The middle loop acts as the velocity loop, facilitating fast and stable control of the mechanism's speed. Lastly, the outer loop functions as the position loop, enabling precise positioning of either distance or angle. The control structure diagram is presented in Figure 8.

$G_i(s)$, $G_v(s)$, $G_p(s)$ are controllers of the current loop, speed loop, and position loop, respectively. The position and speed are given by the system respectively, and their specific values are determined by different scanning steps of the scanner. The position feedback signal comes from the high-precision photoelectric encoder and hysteresis displacement sensor;

The speed signal is obtained by the difference of the position signal and the current feedback signal is collected by the current sensor.

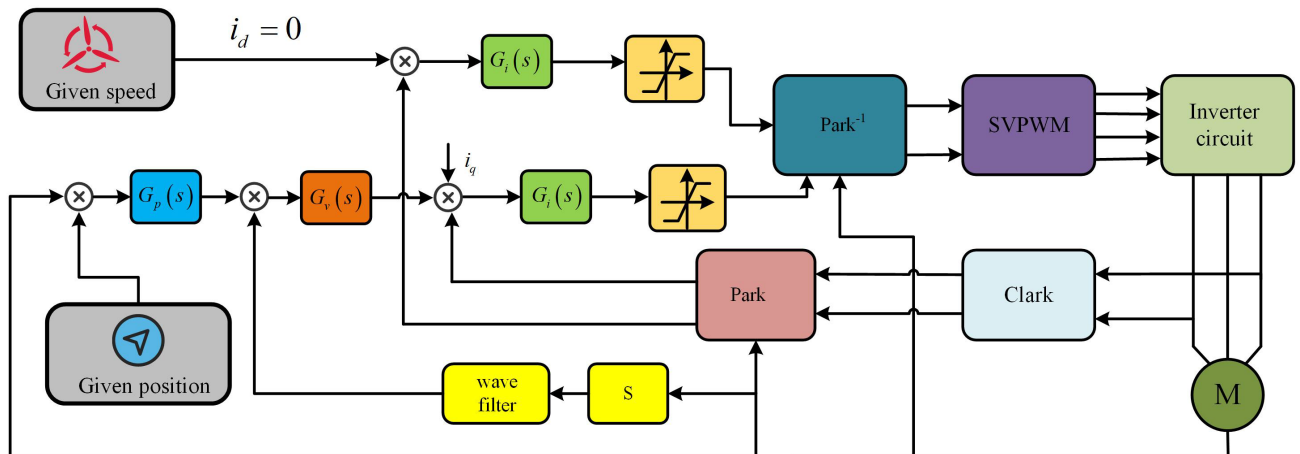


Fig. 8. Control structure block diagram

The permanent magnet synchronous motor adopts the space vector control mode. Because the designed motor is a surface-mounted permanent magnet synchronous motor, its electromagnetic equation in the two-phase rotating coordinate system is:

$$\begin{cases} u_d = R_s i_d + \frac{d\psi_d}{dt} - \omega \psi_q \\ u_q = R_s i_q + \frac{d\psi_q}{dt} + \omega \psi_d \\ \psi_q = L_q i_q \\ \psi_d = L_d i_d + \psi_f \end{cases} \quad (9)$$

Among them, u_d and u_q are the q axis and d axis armature voltage components in the dq coordinate, respectively; i_q and i_d are the q axis and d axis armature current components in the dq coordinate, respectively; R_s is the resistance of the armature winding, ψ_q, ψ_d respectively represent the stator flux components in the dq coordinates; ϕ is the coupling magnetic linkage of the rotor magnetic steel on the stator winding; L_d, L_q respectively represent the equivalent armature inductance components of the q axis and d axis in the dq coordinates.

The kinematic equation of synchronous motor is shown in equation (10)

$$\begin{cases} T_e = \frac{3}{2}n[\phi \cdot i_q + (L_d - L_q)i_q i_d] \\ T_e - T_l = J\omega_e \end{cases} \quad (10)$$

For surface-mounted synchronous motors, $L_d \approx L_q$, Then there is the following relationship:

$$\begin{cases} T_e = \frac{3}{2}n \cdot \psi_f \cdot i_q \\ T_e - T_l = J\omega_e \end{cases} \quad (11)$$

Therefore, for the surface-mounted synchronous motor, the $i_d = 0$ control mode is usually adopted. By controlling the direct axis current i_q , the electromagnetic torque of the synchronous motor can be indirectly controlled, and then the speed and position of the synchronous motor can be controlled.

- Synchronous control of two motors

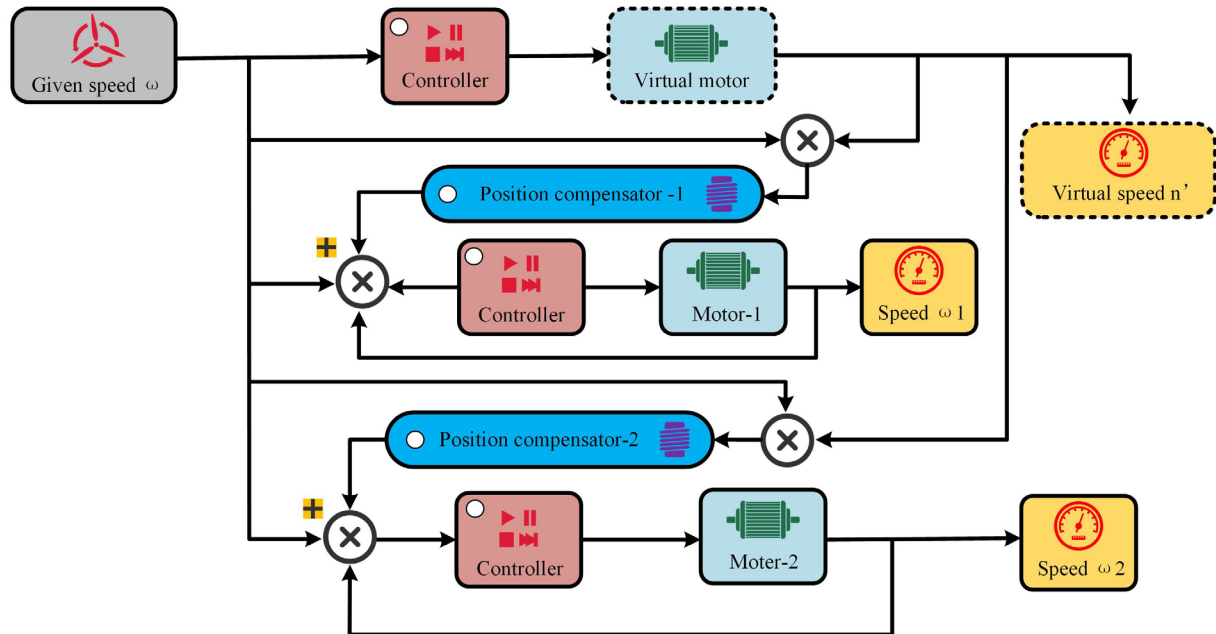


Fig. 9. Master slave coupling synchronous control schematic diagram of virtual spindle

The axial translation and circumferential rotation of the structured-light scanner are driven by a coordinated system of two motors. However, if there exists a significant deviation in the startup timing and rotational cycles between the coordinated motors, it can lead to undesirable mechanical vibrations, jerky movements, or even complete system immobilization. Thus, achieving precise synchronization in motor control is of paramount importance.

The position control mode utilized in this study is based on a position loop, where the feedback for the position loop is derived from the encoder of the servo system. The input to the position loop, together with the feedback signal from the encoder, undergoes computation through a deviation counter. The resulting value is subsequently subjected to adjustment by

the PID controller within the position loop, thus yielding the adjusted output. This adjusted output, in combination with the feed-forward value of the position setpoint, establishes the setpoint for the velocity loop.

To ensure synchronization of the dual-axis servo drive system, an appropriate strategy involves employing a position control mode featuring a virtual master axis. This involves comparing the speeds of the active motor and the passive motor and compensating for the difference by adding it to the control input of either the passive or active motor.

This paper presents a novel design: a virtual master-slave axis position-coupling synchronous control system, as illustrated in Figure 9. Within the motion control system, the controller establishes a virtual axis, with the displacement of this virtual axis being determined by the actual positions of the dual axes. A position coupling synchronous control mode is implemented between the virtual master axis and the slave axis. The fundamental principle of this mode involves calculating the discrepancy between the position feedback of one motor and the position feedback of the other motor. Subsequently, all the discrepancies are summed to obtain the position compensation signal for the respective motor.

By employing the virtual master-slave axis coupling synchronization control, the two motors are intricately linked. Whenever the system load experiences fluctuations that cause changes in the speed of one motor, the other motor promptly adjusts its operating state to ensure the simultaneous operation of both motors, thereby maintaining synchronization between them.

3. Results

The proposed dry-cabin mapping system has been tested and applied in the offshore area near Zhoushan City, Zhejiang Province, during which the pipeline's precise three-dimensional (3D) image is successfully reconstructed. A 12-degree curved submarine pipeline with a length of 12 meters was meticulously welded onto a robust steel platform as the experimental subject, as exemplified in Figure 10. Subsequently, it was meticulously submerged in the designated marine area, followed by carefully hoisting the entire equipment into the sea and spanning it across the test pipeline section.

On the vessel, the remote control was seamlessly achieved utilizing the SLSDS and SECS, combined with the motor synchronous drive technology and tailored strategies for pipeline mapping. Operators seamlessly controlled the motion of the structure-light scanner, facilitating the comprehensive survey of the entire pipeline surface. Real-time feedback from the scanning process allowed for agile adaptation of the scanning strategy, ensuring the complete test pipeline section was scanned.

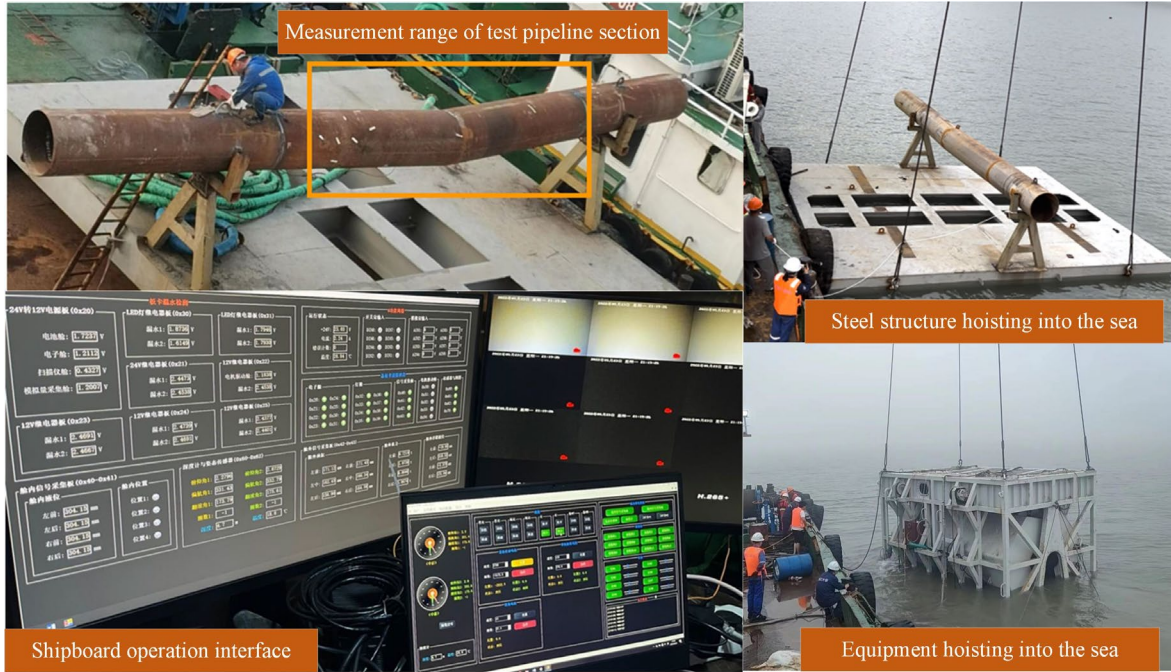


Fig. 10. Test pipeline section and steel platform

The meticulous scanning process, as illustrated in Figure 11, involved the deployment of the structured-light scanner to capture detailed images of the pipeline from different angles, enabling the acquisition of comprehensive point cloud data.



Fig. 11. Test pipeline section and steel platform

The results of processing submarine pipeline structured light data are presented in Figure 12. Due to storage limitations and the nonlinear increase in data processing difficulty with data volume, a stepwise and segmented scanning approach was adopted for the submarine pipeline. Each small segment was formed via continuous scanning with the structured-light scanner, and the specific scanning strategy was implemented according to the preceding chapter. Image stitching between fragments was achieved via feature matching, with the exclusion of partial bad point data and smoothing and filling of a small number of missing data. The resulting comprehensive 3D image accurately depicts the actual state of the tested pipeline on the seafloor.

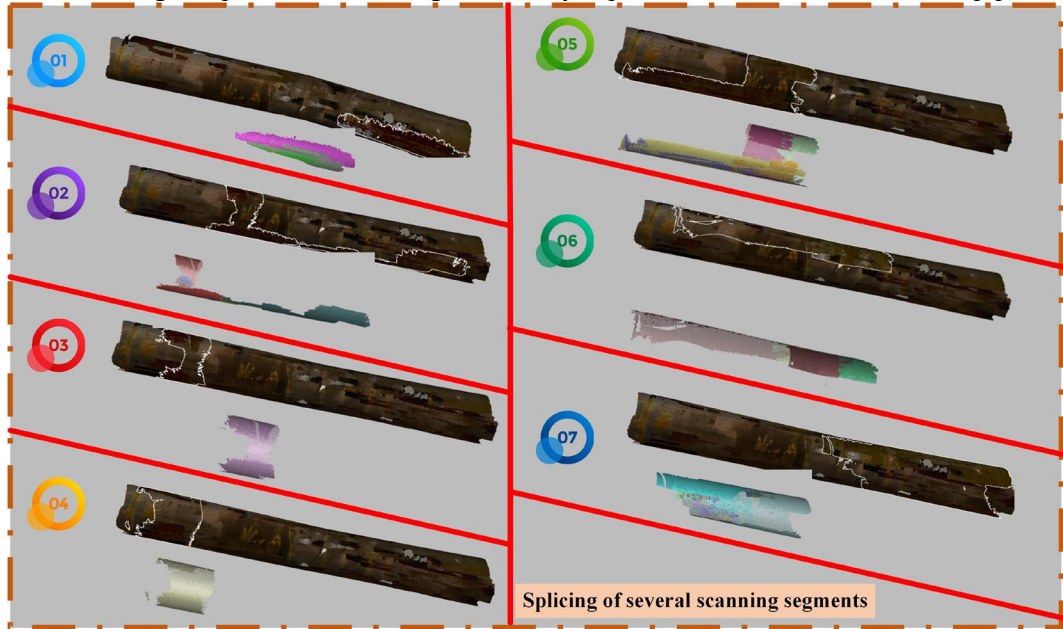


Fig. 12. Scanning fragments and their splicing

Post-processing of the acquired data is a crucial step in structured light scanning. This process involves filtering, noise reduction, and data fusion techniques to enhance the overall quality of the data and minimize any inherent measurement uncertainties. The robustness and reliability of the post-processing algorithms employed significantly contribute to the accuracy of the extracted feature parameters. Additionally, these algorithms play a pivotal role in mitigating any artifacts or distortions introduced during the imaging process, further improving the reliability of the obtained results.

Point cloud data processing software (Artec Studio) was used to store, measure, and analyze the acquired data to achieve the desired results. Artec Studio enables the extraction of feature parameters that comprehensively describe the detected defects or features. Parameters such as size, shape, orientation, and spatial distribution are quantitatively evaluated,

facilitating a detailed understanding of the observed phenomena. This quantitative information can be further utilized to develop mathematical models, perform simulations, and predict the behavior of the pipeline under different operating conditions.

The complete structure of the test pipeline section is finally obtained through the splicing and fusion of point cloud data from the scanner, as shown in Figure 13-A.

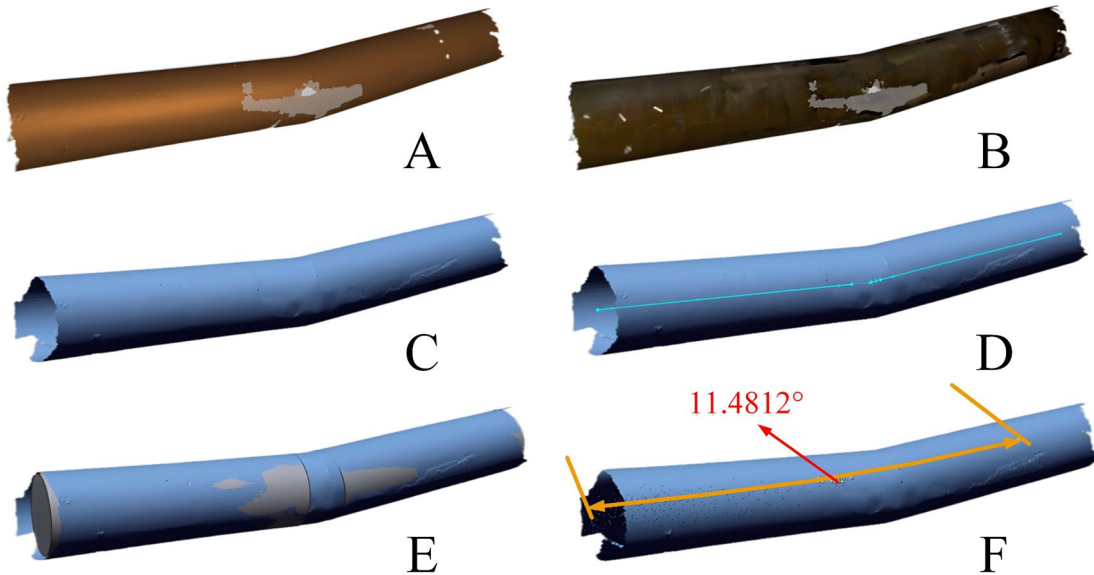


Fig. 13. Post processing of point cloud data in the sea test pipeline section

In the process of 3D scanning, the texture information of the pipe surface is also captured. Combined with the structure diagram, the results in Figure 13-B can be obtained:

The point cloud data denoising technology is used to preprocess the scanning data. In conjunction with interpolation algorithms, missing local point information that is difficult to obtain during the scanning process is filled in. The results after filling are shown in Figure 13-C.

The central point information of the pipeline is derived through a simulation algorithm that combines weighted averaging of parameter information from various points along the circumference of the pipe. In this case, where the pipeline undergoes a transition forming an angular corner, the process involves extracting separate axis lines for the left and right ends. These individual axis lines are fitted together at their intersection to calculate the central axis line information at the corner. The resulting central axis line, depicted in Figure 13-D, spans a total length of 5685.7566 mm within the pipeline.

Based on the information of the central axis and parameters of the test pipeline section, the 3D pipeline trend is inversely reconstructed using cylindrical fitting. The results are shown in Figure 13-E below:

By obtaining the tangent of the central axis of the farthest two end faces, the included angle formed by the two is the calculated coaxial value. The angle value obtained by model calculation is 11.4812° , as shown in Figure 13-F.

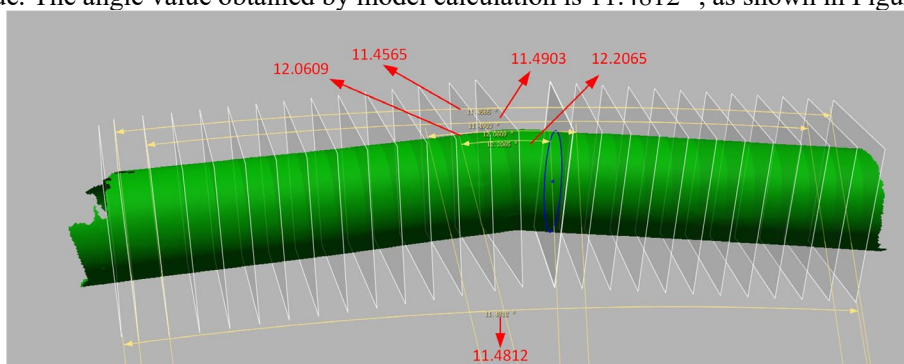


Fig. 14. The angle values measured by four pairs of symmetrical cross-sections at different distances

Along the trend of the central axis of the pipeline section, cut off several planes perpendicular to the central axis, select four sets of symmetrical planes at different positions from the inflection point, and measure the corresponding angle values. The obtained results are 11.4565° , 11.4903° , 12.0609° , and 12.2065° , respectively. The location diagram is shown in Figure 14:

According to the above analysis, the conclusions of the 3D scanning measurement of the 12° pipe section are as follows:

- (1) The scanning range is 5685.7566mm along the axis;
- (2) According to the measured data obtained by 3D scanning, the numerical calculation was carried out, and the coaxiality of the end face was 11.4812° ;

(3) The orientation of the bending apex: the vertical direction is 12 o'clock, and the axis is outward along the hull. It protrudes at about 9 o'clock.

In general, the damage of energy pipelines is mainly corrosion and fracture. Such damaged surfaces are irregular shapes. At the same time, it is impossible to directly measure the degree of damage, such as the depth and thickness after corrosion. The traditional measurement method has high requirements for operators, and there are some manual operation errors. Structured light mapping makes up for the above defects.

Utilizing local magnification techniques to enhance the visibility of specific features or defects in submarine pipelines is of great significance in providing crucial references for defect repairs. This approach allows for a detailed examination of localized areas of interest by leveraging point cloud data processing software, enabling efficient storage, accurate measurement, and extraction of essential feature parameters. The advantages of structured light scanning in this context are manifold, encompassing digitalized data storage, versatile editing capabilities, comprehensive post-processing functionalities, and the assurance of measurement precision.

One of the primary benefits of employing structured light scanning is its ability to achieve high-resolution imaging of submarine pipelines. The surface weld can be clearly seen from the locally enlarged scanning pipe section, as shown in Figure 15. Even subtle features or defects that may otherwise go unnoticed can be effectively highlighted using local magnification. This technique plays a vital role in identifying and characterizing various types of imperfections, such as cracks, corrosion, deformations, or joint misalignments, which can compromise the integrity and functionality of the pipelines. The ability to accurately visualize these flaws is paramount for planning and executing efficient repair strategies, as it allows for targeted interventions.

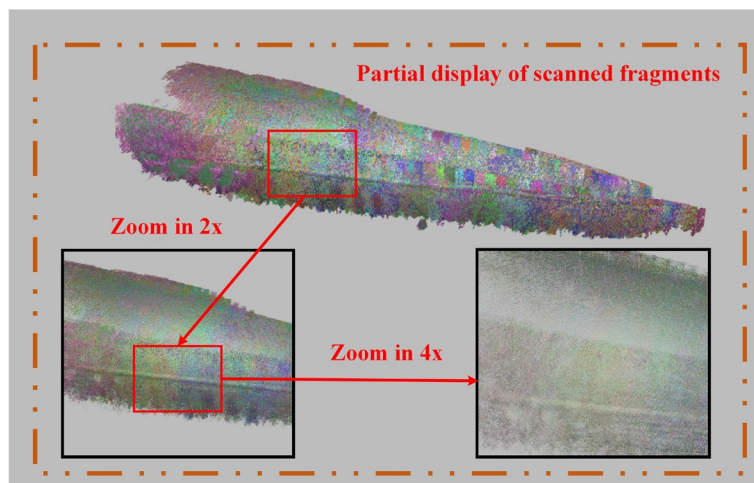


Fig. 15. Enlarged display of details of point cloud data

4. Discussion

The utilization of structured light photometry in this study has demonstrated its high precision, enabling local magnification and clear visualization of surface features, including the weld seam on the submarine pipeline. Through a comprehensive inspection of the entire pipe section, hazardous points were identified for further analysis and treatment, enabling the assessment of pipe damage, deformation, bending, and corrosion. Structured light photometry offers distinct advantages in high-density data acquisition and the extraction of multiple feature parameters, surpassing alternative techniques in these domains. The obtained data is quantifiable, editable, and characterized by exceptional accuracy, highlighting its significance in pipeline inspection. Structured light mapping ensures the digitization of pipeline inspection data, enabling efficient storage and convenient access for subsequent analysis and decision-making processes. The digital

nature of the data allows for easy sharing, collaboration, and integration with other inspection and maintenance systems. Furthermore, it facilitates the development of databases for long-term monitoring and trend analysis, contributing to the establishment of proactive maintenance strategies and the optimization of pipeline management.

The successful implementation of structured light scanning for submarine pipeline inspection heavily relies on the establishment of dry chambers on the seafloor. To address this challenge, our study integrates two complementary technologies to leverage the high-precision capabilities of structured light for submarine pipeline mapping.

In this paper, our focus lies on the research and development of the structured light scanning drive mechanism. While motor synchronous drive technology ensures minimal deviations in drive time and accuracy, occasional jerky movements during prolonged scanning operations may arise due to inherent design flaws in the mechanical structure. Therefore, a key area for future research involves the development of an innovative drive structure for the scanner, offering enhanced convenience and smoother movements. This advancement would minimize disruptions and optimize the efficiency of the scanning process.

To further enhance the performance of structured light scanning in submarine pipeline inspection, several aspects warrant optimization:

1. Commercially available structured-light scanners, while convenient for integration, may not be specifically designed for scanning outside submarine pipelines. Overcoming this limitation requires addressing several factors. First, improving the sealing performance of the scanner is essential to ensure reliable operation in challenging underwater environments. Second, enhancing the ease of installation would expedite deployment. Third, incorporating functionality to eliminate water droplets on the scanner's surface would result in clearer imaging. Lastly, strengthening the convenience of remote operation would facilitate efficient data acquisition.

2. Strengthening the technical principles underlying structured light scanning should be a focus of future research efforts. This can be achieved through the development of a new submarine pipeline scanning scheme that disperses the structured light scanning lenses within the dry chambers. By doing so, the need for frequent position switching, which can introduce errors, would be reduced. Additionally, adaptive improvements to the imaging algorithms employed in structured light scanning can better accommodate the specific conditions encountered during submarine pipeline inspections.

3. The integration of other intelligent devices, such as unmanned aerial vehicles (UAVs) and robotic arms, can significantly enhance the automation level of the scanning process. UAVs offer an aerial perspective, enabling a broader view of the submarine pipeline and facilitating more efficient data collection. Robotic arms, on the other hand, can be utilized for precise positioning and manipulation of the structured-light scanner, ensuring accurate and repeatable measurements.

4. Enhancing image processing capabilities plays a crucial role in structured light scanning. Advanced image processing techniques should be employed to analyze defect characteristics accurately. By conducting comparative analyses between the defect features extracted from the images and the corresponding structured light scanning data, the overall accuracy and reliability of structured light scanning can be further substantiated. This approach not only enhances confidence in defect identification but also provides valuable insights for further optimization of the technique.

5. Conclusions

Our study represents an innovation in the field of submarine pipeline inspection, presenting a bold and novel approach that combines dry cabin technology and structured light mapping. This pioneering method has overcome the challenges posed by seawater interference and leverages the precision and convenience of structured light technology in pipeline mapping. Moreover, the implementation of dry cabin technology for submarine pipelines, the first of its kind in China, demonstrates an innovative application with significant potential.

The development of the SLSDS has facilitated precise scanning range calculation and the formulation of suitable scanning strategies for pipelines. Additionally, we have designed a comprehensive SECS, providing a holistic solution for power supply, sensing, communication, and control during the inspection process.

Extensive research has been conducted on the synchronization control of multiple motors, leading to the implementation of a virtual master-slave axis position coupling synchronization control system. This system ensures seamless propulsion during pipeline scanning, minimizing disruptions and maximizing data quality. By integrating point cloud data processing software, we have achieved precise and detailed 3D representations of the external surfaces of 5685mm-long submarine pipelines.

The results of our study demonstrate exceptional pipeline scanning accuracy, reaching an impressive level of 0.1mm. This high level of accuracy is applicable even in marine areas with varying levels of visibility. The proposed technical solution

represents an advancement in the field of external pipeline inspection, providing an efficient and reliable method for the accurate assessment of pipeline damage.

Accurate and effective assessment of pipeline damage is critical for the long-term maintenance of pipeline networks in offshore oil and gas operations. By enabling external inspection, our approach significantly enhances the safety and reliability of these operations. The detailed 3D representations obtained through structured light scanning provide valuable insights into the condition of submarine pipelines, enabling proactive maintenance and timely repair of any detected defects.

In conclusion, our study introduces an innovative approach that combines structured light technology with underwater dry chamber technology, enabling accurate and effective external inspection of submarine pipelines. The achieved level of accuracy, along with the proposed technical solution, has the potential to form a certain degree of supplement to the field of pipeline inspection and maintenance. The advancements made in scanning accuracy contribute to the overall safety, reliability, and long-term sustainability of offshore oil and gas operations, especially demonstrating its potential to be widely used in sea areas with poor-visibility underwater conditions.

Acknowledgments

This work was funded by the Pipe China Eastern Crude Oil Storage and Transportation Co., Ltd. (No. GWHT20220003812), and the Major Cooperative Projects of Zhejiang Province Market Supervision and Administration (No. CY2023107).

References

- [1] Fang H., Duan M., Chapter 6 - Submarine Pipelines and Pipeline Cable Engineering, in: Fang H., Duan M. (Eds.), Offshore Oper. Facil., Gulf Professional Publishing, Boston, 2014: pp. e1–e181. <https://doi.org/10.1016/B978-0-12-396977-4.00006-8>.
- [2] H. Lu, T. Iseley, S. Behbahani, L. Fu, Leakage detection techniques for oil and gas pipelines: State-of-the-art, *Tunn. Undergr. Space Technol.* 98 (2020) 103249. <https://doi.org/10.1016/j.tust.2019.103249>.
- [3] H. Lu, L. Guo, M. Azimi, K. Huang, Oil and Gas 4.0 era: A systematic review and outlook, *Comput. Ind.* 111 (2019) 68–90. <https://doi.org/10.1016/j.compind.2019.06.007>.
- [4] H. Lu, L. Guo, Y. Zhang, Oil and gas companies' low-carbon emission transition to integrated energy companies, *Sci. Total Environ.* 686 (2019) 1202–1209. <https://doi.org/10.1016/j.scitotenv.2019.06.014>.
- [5] H. Lu, K. Huang, M. Azimi, L. Guo, Blockchain Technology in the Oil and Gas Industry: A Review of Applications, Opportunities, Challenges, and Risks, *IEEE Access.* 7 (2019) 41426–41444. <https://doi.org/10.1109/ACCESS.2019.2907695>.
- [6] M. Khajouei, S. Khamani, K. Adavi, Chapter Five - Wall thinning and damage detection techniques in pipelines, in: V. Kushvaha, S. Mavinkere Rangappa, G. Balaganesan, S. Siengchin (Eds.), *Polym. Compos. Syst. Pipeline Repair*, Gulf Professional Publishing, 2023: pp. 93–106. <https://doi.org/10.1016/B978-0-323-99340-1.00005-8>.
- [7] J. Wang, R. He, H. Zhang, H. Guo, Q. Wu, State-of-the-art Advancement and Development Direction of Submarine Pipeline Inspection Technology, *China Pet. Mach.* 44 (2016) 112–118. <https://doi.org/10.16082/j.cnki.issn.1001-4578.2016.10.025>.
- [8] B. Liu, Y. Liang, L. He, Z. Lian, H. Geng, L. Yang, Quantitative study on the propagation characteristics of MFL signals of outer surface defects in long-distance oil and gas pipelines, *NDT E Int.* 137 (2023) 102861. <https://doi.org/10.1016/j.ndteint.2023.102861>.
- [9] Peng X., Anyaoha U., Liu Z., Tsukada K., Analysis of Magnetic-Flux Leakage (MFL) Data for Pipeline Corrosion Assessment, *IEEE Trans. Magn.* 56 (2020) 1–15. <https://doi.org/10.1109/TMAG.2020.2981450>.
- [10] Zhao K., Xinjun W., Shen G., A Portable Magnetic Flux Leakage Testing System for Industrial Pipelines Based on Circumferential Magnetization, in: 2016. <https://www.semanticscholar.org/paper/A-Portable-Magnetic-Flux-Leakage-Testing-System-for-Zhao-Xinjun/0f9e70b959ab020d50279882054e83574b1251df> (accessed June 5, 2023).
- [11] H. Liang, G. Cheng, Z. Zhang, H. Yang, Research on ultrasonic defect identification method of well control manifold pipeline based on IAFSA-SVM, *Measurement.* 194 (2022) 110854. <https://doi.org/10.1016/j.measurement.2022.110854>.
- [12] J. Yuan, W. Mao, C. Hu, J. Zheng, D. Zheng, Y. Yang, Leak detection and localization techniques in oil and gas pipeline: A bibliometric and systematic review, *Eng. Fail. Anal.* 146 (2023) 107060. <https://doi.org/10.1016/j.engfailanal.2023.107060>.
- [13] T. Hu, J. Guo, Development and application of new technologies and equipment for in-line pipeline inspection, *Nat. Gas Ind. B.* 6 (2019) 404–411. <https://doi.org/10.1016/j.ngib.2019.01.017>.
- [14] M. Xie, Z. Tian, A review on pipeline integrity management utilizing in-line inspection data, *Eng. Fail. Anal.* 92 (2018) 222–239. <https://doi.org/10.1016/j.engfailanal.2018.05.010>.
- [15] B.T. Bastian, J. N, S.K. Ranjith, C.V. Jiji, Visual inspection and characterization of external corrosion in pipelines using deep neural network, *NDT E Int.* 107 (2019) 102134. <https://doi.org/10.1016/j.ndteint.2019.102134>.
- [16] Chen W., Liu Z., Zhang H., Chen M., Zhang Y., A submarine pipeline segmentation method for noisy forward-looking sonar images using global information and coarse segmentation, *Appl. Ocean Res.* 112 (2021) 102691. <https://doi.org/10.1016/j.apor.2021.102691>.

-
- [17] W.J.S. Gomes, A.T. Beck, T. Haukaas, Optimal inspection planning for onshore pipelines subject to external corrosion, *Reliab. Eng. Syst. Saf.* 118 (2013) 18–27. <https://doi.org/10.1016/j.ress.2013.04.011>.
- [18] H.P. Hong, Inspection and maintenance planning of pipeline under external corrosion considering generation of new defects, *Struct. Saf.* 21 (1999) 203–222. [https://doi.org/10.1016/S0167-4730\(99\)00016-8](https://doi.org/10.1016/S0167-4730(99)00016-8).
- [19] Zhang H., Zhang S., Wang Y., Liu Y., Yang Y., Zhou T., Bian H., Subsea pipeline leak inspection by autonomous underwater vehicle, *Appl. Ocean Res.* 107 (2021) 102321. <https://doi.org/10.1016/j.apor.2020.102321>.
- [20] Zhang Y., Zhang H., Liu J., Zhang S., Liu Z., Lyu E., Chen W., Submarine pipeline tracking technology based on AUVs with forward looking sonar, *Appl. Ocean Res.* 122 (2022) 103128. <https://doi.org/10.1016/j.apor.2022.103128>.
- [21] J.B. Cunha, A.A. Neto, Ultrahigh-resolution seismic enhancement. The use of colored inversion and seismic attributes on sub-bottom profiler data, *J. Appl. Geophys.* 184 (2021) 104184. <https://doi.org/10.1016/j.jappgeo.2020.104184>.
- [22] W. Zhang, T. Zhou, D. Peng, J. Shen, Underwater pipeline leakage detection via multibeam sonar imagery, *J. Acoust. Soc. Am.* 141 (2017) 3917. <https://doi.org/10.1121/1.4988849>.
- [23] Y. Chen, H. Li, Y. Yao, P. Yang, X. Ye, S. Xiao, Submarine Pipeline Identification in Side Scan Sonar Image, in: 2018 IEEE Int. Conf. Mechatron. Autom. ICMA, 2018: pp. 2109–2114. <https://doi.org/10.1109/ICMA.2018.8484417>.
- [24] H. Feng, J. Yu, Y. Huang, J. Cui, J. Qiao, Z. Wang, Z. Xie, K. Ren, Automatic tracking method for submarine cables and pipelines of AUV based on side scan sonar, *Ocean Eng.* 280 (2023) 114689. <https://doi.org/10.1016/j.oceaneng.2023.114689>.
- [25] L. Jing, The principle of side scan sonar and its application in the detection of suspended submarine pipeline treatment, *IOP Conf. Ser. Mater. Sci. Eng.* 439 (2018) 032068. <https://doi.org/10.1088/1757-899X/439/3/032068>.
- [26] M.A. Pasha, T.M. Khan, A pipeline inspection gauge based on low cost magnetic flux leakage sensing magnetometers for non-destructive testing of pipelines, in: 2016 Int. Conf. Emerg. Technol. ICET, 2016: pp. 1–5. <https://doi.org/10.1109/ICET.2016.7813212>.
- [27] Wan Y., Wang Y., Yang Y., Liu C., Dai Y., Intelligent identification and classification methods of oil and gas pipeline defects by fluxgate magnetometry, *Harbin Gongcheng Daxue Xuebao.* 42 (2021) 1321–1329. <https://doi.org/10.11990/jheu.202005049>.
- [28] Y. Li, Q. Liu, Y. Chen, M. Li, HELICAL-CONTACT DEFORMATION MEASURING METHOD IN OIL-GAS PIPELINES, in: *Int. J. Robot. Autom.* 2017, ACTA Press, 2017. <https://doi.org/10.2316/Journal.206.2017.1.206-4772>.
- [29] Y. Chen, Y. Kang, B. Feng, Y. Li, X. Cai, S. Wang, Automatic defect identification in magnetic particle testing using a digital model aided De-noising method, *Measurement.* 198 (2022) 111427. <https://doi.org/10.1016/j.measurement.2022.111427>.
- [30] P.J. Kentish, Gas pipeline failures: Australian experience, *Br. Corros. J.* 20 (1985) 139–146. <https://doi.org/10.1179/000705985798272786>.
- [31] M. Coramik, Y. Ege, Discontinuity inspection in pipelines: A comparison review, *Measurement.* 111 (2017) 359–373. <https://doi.org/10.1016/j.measurement.2017.07.058>.
- [32] M.M.M. Nadzri, A. Ahmad, Design Issues and Challenges of Long-Range Ultrasonic Testing (LRUT) for Pipeline Inspection, in: K. Isa, Z. Md. Zain, R. Mohd-Mokhtar, M. Mat Noh, Z.H. Ismail, A.A. Yusof, A.F. Mohamad Ayob, S.S. Azhar Ali, H. Abdul Kadir (Eds.), *Proc. 12th Natl. Tech. Semin. Unmanned Syst. Technol.* 2020, Springer, Singapore, 2022: pp. 115–126. https://doi.org/10.1007/978-981-16-2406-3_10.
- [33] S. She, Y. Chen, Y. He, Z. Zhou, X. Zou, Optimal design of remote field eddy current testing probe for ferromagnetic pipeline inspection, *Measurement.* 168 (2021) 108306. <https://doi.org/10.1016/j.measurement.2020.108306>.
- [34] X.-F. Li, J. Sun, S. Lu, L. Wang, Application of On-line Digital Radiographic Inspection for Pipeline with Insulation, *J. Phys. Conf. Ser.* 2366 (2022) 012006. <https://doi.org/10.1088/1742-6596/2366/1/012006>.

-
- [35] Zhao S., Shen Y., Sun L., Wang J., Mao Z., Chu Z., Chen J., Gao J., A method to compensate for the lift off effect of ACFM in crack estimation of nonferromagnetic metals, *J. Magn. Magn. Mater.* 554 (2022) 169301. <https://doi.org/10.1016/j.jmmm.2022.169301>.
- [36] Wan Abdullah Zawawi N.A., Liew M.S., Alaloul W., Lim E.S., Imran M., Toloue I., Non-Destructive Testing Techniques for Offshore Underwater Decommissioning Projects through Cutting Detection: A State of Review, 2019. <https://doi.org/10.2118/199191-MS>.
- [37] Smith M., Sutherby R., The detection of pipeline SCC flaws using the ACFM technique, *Insight - Non-Destr. Test. Cond. Monit.* 47 (2005) 765–768. <https://doi.org/10.1784/insi.2005.47.12.765>.
- [38] Forbes A., Structured Light from Lasers, *Laser Photonics Rev.* 13 (2019) 1900140. <https://doi.org/10.1002/lpor.201900140>.
- [39] A. Forbes, M. de Oliveira, M.R. Dennis, Structured light, *Nat. Photonics.* 15 (2021) 253–262. <https://doi.org/10.1038/s41566-021-00780-4>.
- [40] Geng J., Structured-light 3D surface imaging: a tutorial, *Adv. Opt. Photonics.* 3 (2011) 128–160. <https://doi.org/10.1364/AOP.3.000128>.
- [41] Giancola S., Valenti M., Sala R., A Survey on 3D Cameras: Metrological Comparison of Time-of-Flight, Structured-Light and Active Stereoscopy Technologies, Springer International Publishing, Cham, 2018. <https://doi.org/10.1007/978-3-319-91761-0>.
- [42] Kim G., Kim Y., Yun J., Moon S.-W., Kim S., Kim J., Park J., Badloe T., Kim I., Rho J., Metasurface-driven full-space structured light for three-dimensional imaging, *Nat. Commun.* 13 (2022) 5920. <https://doi.org/10.1038/s41467-022-32117-2>.
- [43] Wang J., Liang Y., Generation and Detection of Structured Light: A Review, *Front. Phys.* 9 (2021). <https://www.frontiersin.org/articles/10.3389/fphy.2021.688284> (accessed September 12, 2022).
- [44] L.-S. Bieri, J. Jacot, Three-dimensional vision using structured light applied to quality control in production line, in: *Opt. Metrol. Prod. Eng.*, SPIE, 2004: pp. 463–471. <https://doi.org/10.1117/12.545039>.
- [45] Cao X., Xie W., Ahmed S.M., Li C.R., Defect detection method for rail surface based on line-structured light, *Measurement.* 159 (2020) 107771. <https://doi.org/10.1016/j.measurement.2020.107771>.
- [46] M. Schaffer, M. Grosse, B. Harendt, R. Kowarschik, High-speed three-dimensional shape measurements of objects with laser speckles and acousto-optical deflection, *Opt. Lett.* 36 (2011) 3097–3099. <https://doi.org/10.1364/OL.36.003097>.
- [47] Z. Wang, S. Liu, J. Hu, W. Zhang, H. Huang, J. Liu, Line structured light 3D measurement technology for pipeline microscratches based on telecentric lens, *Opt. Eng.* 60 (2021) 124108. <https://doi.org/10.1117/1.OE.60.12.124108>.
- [48] L.K. e Silva, G. Almeida, C. Nunes, G.R. Pereira, D. Kadoke, W. Daum, Automation of pipe defect detection and characterization by structured light, *Mater. Test.* 63 (2021) 55–61. <https://doi.org/10.1515/mt-2020-0008>.
- [49] W. Ying, J. Cuiyun, Z. Yanhui, Pipe Defect Detection and Reconstruction Based on 3D Points Acquired by the Circular Structured Light Vision, *Adv. Mech. Eng.* 5 (2013) 670487. <https://doi.org/10.1155/2013/670487>.
- [50] Leroux T., Ieng S.-H., Benosman R., Event-Based Structured Light for Depth Reconstruction using Frequency Tagged Light Patterns, 2018.
- [51] Wu Z., Guo W., Zhang Q., Wang H., Li X., Chen Z., Time-overlapping structured-light projection: high performance on 3D shape measurement for complex dynamic scenes, *Opt. Express.* 30 (2022) 22467–22486. <https://doi.org/10.1364/OE.460088>.
- [52] Ye J., Zhou C., Time-resolved coded structured light for 3D measurement, *Microw. Opt. Technol. Lett.* 63 (2021) 5–12. <https://doi.org/10.1002/mop.32548>.
- [53] Cui H., Liao W., Dai N., Cheng X., A flexible and rapid micro-adjustment algorithm for structured light 3D measurement system with camera-projector, *Optik.* 123 (2012) 109–116. <https://doi.org/10.1016/j.jleo.2011.03.008>.

-
- [54] Wang Q.-H., Ni P.-N., Xie Y.-Y., Kan Q., Chen P.-P., Fu P., Deng J., Jin T.-L., Chen H.-D., Lee H.W.H., Xu C., Genevet P., On-Chip Generation of Structured Light Based on Metasurface Optoelectronic Integration, *Laser Photonics Rev.* 15 (2021) 2000385. <https://doi.org/10.1002/lpor.202000385>.
- [55] Sun P.-P., Xue Q., Ji W., Meng H., Sun X., Yang X., Analysis and compensation of lateral chromatic aberration of structured light 3D measurement system, *Opt. Commun.* 488 (2021) 126871. <https://doi.org/10.1016/j.optcom.2021.126871>.
- [56] Li B., An Y., Cappelleri D., Xu J., Zhang S., High-accuracy, high-speed 3D structured light imaging techniques and potential applications to intelligent robotics, *Int. J. Intell. Robot. Appl.* 1 (2017) 86–103. <https://doi.org/10.1007/s41315-016-0001-7>.
- [57] Zhang S., High-speed 3D shape measurement with structured light methods: A review, *Opt. Lasers Eng.* 106 (2018) 119–131. <https://doi.org/10.1016/j.optlaseng.2018.02.017>.
- [58] Liu S., Zhang Y., Zhang Y., Shao T., Yuan M., Research on 3D measurement model by line structure light vision, *EURASIP J. Image Video Process.* 2018 (2018) 88. <https://doi.org/10.1186/s13640-018-0330-6>.
- [59] Ye Z., Lianpo W., Yonggang G., Songlin B., Chao Z., Jiang B., Ni J., Three-Dimensional Inner Surface Inspection System Based on Circle-Structured Light, *J. Manuf. Sci. Eng.* 140 (2018). <https://doi.org/10.1115/1.4041480>.